

AARHUS UNIVERSITY

MASTER'S THESIS

---

**Beta-decay of  $^8\text{Li}$ : beta-alpha correlations  
and final state distribution**

---

*Author:*

Anders Holst Rasmussen

*Supervisor:*

Hans O. U. Fynbo

June 8, 2021



# Contents

<b>1</b>	<b>Introduction</b>	<b>1</b>
1.1	Motivation . . . . .	1
1.2	Nuclear decays . . . . .	2
1.2.1	$\beta$ -decay . . . . .	2
1.2.2	$\alpha$ -decay . . . . .	3
1.3	Structure of $^8\text{Be}$ . . . . .	4
<b>2</b>	<b>Experimental Methods</b>	<b>6</b>
2.1	Detector setup . . . . .	6
2.2	Experimental setup . . . . .	6
2.3	The detectors . . . . .	8
2.4	AUSAlib and ROOT . . . . .	10
2.4.1	Unpacker . . . . .	11
2.4.2	Calibrator . . . . .	11
2.4.3	Sorter . . . . .	13
<b>3</b>	<b>Data Reduction</b>	<b>14</b>
3.1	Calibration . . . . .	14
3.2	Identifying the particles . . . . .	15
3.2.1	Identifying a hit . . . . .	16
3.3	Angular cut . . . . .	17
3.4	Momentum cut . . . . .	18
3.5	Multiplicity cut . . . . .	19
<b>4</b>	<b>Analysis</b>	<b>21</b>
4.1	The effects of the cuts . . . . .	21
4.1.1	The effect of the angular cut . . . . .	23
4.1.2	The effect of the momentum cut . . . . .	23

4.1.3	The effect of the multiplicity cut . . . . .	24
4.1.4	The combined effect of all the cuts . . . . .	24
4.2	The excitation energy of $^8\text{Be}$ . . . . .	25
4.3	Angular efficiency of the setup . . . . .	26
4.4	Angular correlations of $\alpha$ -particles and $\beta$ -particles . . . . .	31
<b>5</b>	<b>Conclusion</b>	<b>35</b>

# 1 Introduction

## 1.1 Motivation

When Henri Becquerel first discovered radioactivity in the 1890's, a new branch of atomic physics was born, namely nuclear physics, which is the study of the atomic nuclei, their constituents and interactions. Over the years it has evolved quickly, first by the discovery of three different types of radiation by Curie and Rutherford, to the discovery of different nucleons, that the nucleus itself is made of. [måske ref til Curie and Rutherford?](#)

The technological advancements has made the study even more precise over the years, as the development of radioactive beams allow for the creation of specific short lived isotopes. This technique is known as Isotope Separation On-Line (ISOL), which was first developed in 1951 for the Copenhagen Cyclotron. Now the technology is available in many parts of the world, such as the IGISOL facility at the University of Jyväskylä in Finland. [Måske link til hjemmeside eller noget](#) Another important advancement is the development of very precise detectors, such as the Double Sided Silicon Detector (DSSD), which allows for a very high energy and spacial resolution, which can give a detailed analysis of both coincidence and kinematics.

This brings us onto the current experiment that I have analyzed in this thesis. At the IGISOL facility, the experiment I257 was carried out in august 2020. The objective of the experiment was to measure  $\beta$ -decays from  $^8\text{Li}$  and  $^{12}\text{B}$ , however, this thesis will only govern the  $^8\text{Li}$  decay.

[Man ved måske ikke helt hvad beta-alfa er her](#) The  $\beta$ - $\alpha$  angular correlation is previously shown with high precision to be nearly isotropic [1]. The study of the  $\beta$ - $\alpha$  correlation in  $^8\text{Li}$  will therefore serve as a good indicator for the

$\beta$ - $\alpha$  correlation in  $^{12}\text{B}$ , as the same setup will be used for both experiments. A former student has previously made an in depth analysis of the mirror nucleus  $^8\text{B}$ , which can be used to compare the excitation energy of  $^8\text{Be}$ . A comparison of the two is unfortunately out of scope for this thesis **Måske referer til former student - spørg Hans hvordan.**

## 1.2 Nuclear decays

Lithium normally occurs stable as  $^6\text{Li}$  and  $^7\text{Li}$ , with the latter being the more abundant with 92.5% of all atoms. The longest living radioactive lithium isotope is  $^8\text{Li}$ , with a half-life of 839ms **ref.** When  $^8\text{Li}$  decays, it will do so under a **by i stedet for under a?**  $\beta$ -decay, immediately followed by the  $\alpha$ - $\alpha$  breakup of an intermediate excited state in  $^8\text{Be}$ , which has a half life of  $1 \times 10^{-16}\text{s}$ .  $^8\text{Be}$  is a constituent in the triple-alpha process in stellar astrophysics, and creates a bottleneck for the creation of heavier elements, because of its very short lifespan.

### 1.2.1 $\beta$ -decay

Most light unstable nuclei will decay by either proton/neutron emission, or by a  $\beta$ -decay. Isotopes that lie close to the valley of stability will not decay by proton/neutron emission, but from a  $\beta$ -decay.

A  $\beta$ -decay is a weak interaction, which allows a quark in a proton or neutron to change flavor, by emitting a W boson. This leads to the creation of either an electron/antineutrino pair or a positron/neutrino pair, shown as **måske slet shown as?:**

$$\beta^+ : \quad p \rightarrow n + e^+ + \nu_e \quad (1.1)$$

$$\beta^- : \quad n \rightarrow p + e^- + \bar{\nu}_e. \quad (1.2)$$

Nuclei below the valley of stability will decay by  $\beta^-$ , while nuclei above decays by  $\beta^+$ .

The energy for **of these decays** these decays are given by their Q-values, ne-

glecting the very small neutrino mass and the binding energy of the electrons gives:

$$Q_{\beta^+} = [m({}_Z^AX) - m({}_{Z-1}^AX')] c^2 \quad (1.3)$$

$$Q_{\beta^-} = [m({}_Z^AX) - m({}_{Z+1}^AX') - 2m_e] c^2, \quad (1.4)$$

where  $m$  is the mass of an atom with  $Z$  protons and  $A$  nucleons. The  $Q$ -values indicates the mass difference between the initial and final product., which can be either excitation energy or kinetic energy.

Not all  $\beta$ -decays are allowed. If the spin is unchanged, it is a Fermi transition, and if it changes it is a Gamow-Teller transition. An allowed decay is a transition with the orbital angular momentum  $L = 0$ , and forbidden transitions is  $L > 0$ .

The nuclear part of the  $\beta$ -decay operator for an allowed decay is:

$$\mathcal{O}(\beta^\pm) = g_V \sum_A^{j=1} \tau_\mp(j) + g_A \sum_A^{j=1} \sigma(j) \tau_\mp(j), \quad (1.5)$$

where  $g_V$  is weak vector coupling constant,  $\tau_\mp$  is the isospin step operator,  $g_A$  is the weak axial coupling constant and  $\sigma$  is the Pauli spin matrices. The first term corresponds to the Fermi operator, and the second term to the Gamow-Teller operator. This raises some selection rules, that dictate that for a Fermi decay, spin, isospin and parity must not be changed, and for a Gamow-Teller transitions,  $\Delta J = 0, \pm 1$ ,  $\Delta T = 0, \pm 1$ , and  $\Delta \pi = 0$ .

The selection rules then enforces that not every energy level is populated in  ${}^8\text{Be}$ .

### 1.2.2 $\alpha$ -decay

$\alpha$ -decay is another type of radioactive decay, where the nucleus emits an  $\alpha$ -particle, and thereby decays into a different nucleus with the atomic number reduced by two. It has a  $Q$ -value of:

$$Q_\alpha = [m({}_Z^AX) - m({}_{Z-2}^{A-4}X') - m_\alpha] c^2. \quad (1.6)$$

Usually it is only elements heavier than nickel that can decay via this process, as the binding energy per nucleon decreases, and therefore becomes unstable towards spontaneous fission type processes. The only known exception to this rule is then  ${}^8\text{Be}$ , which is the only light nuclei that decays by  $\alpha$ -decay.

### 1.3 Structure of ${}^8\text{Be}$

Figure 1.1 shows the excitation spectrum for  ${}^8\text{Be}$ , with values from [2]. The spin, parity and isospin are written as  $J^\pi; T$  for each level. 4 different states has been shown for  ${}^8\text{Be}$ , where only the first excited state is the broad state at 3.03 MeV. This state has conservation of spin and parity from  ${}^8\text{Li}$  and is the only state that is allowed for the decay of  ${}^8\text{Li}$ . **Situated** above is the broad state at 11.35 MeV, which does not conserve spin. Above that is a 16.626 MeV state, which conserves spin, parity and isospin, but lies energetically above  ${}^8\text{Li}$ , so we would not expect that to shown in the data. It is still a quite relevant state, as the mirror nucleus  ${}^8\text{B}$  ( $2^+; 1$ ) lies just above the energy at 17.979 MeV, and then has enough energy to populate this state, even though it is not very likely. Previous experiments made by the Aarhus subatomic group has examined the decay, and found only 5 counts populating this excitation level. But that should not show up when looking at the decay of  ${}^8\text{Li}$ .

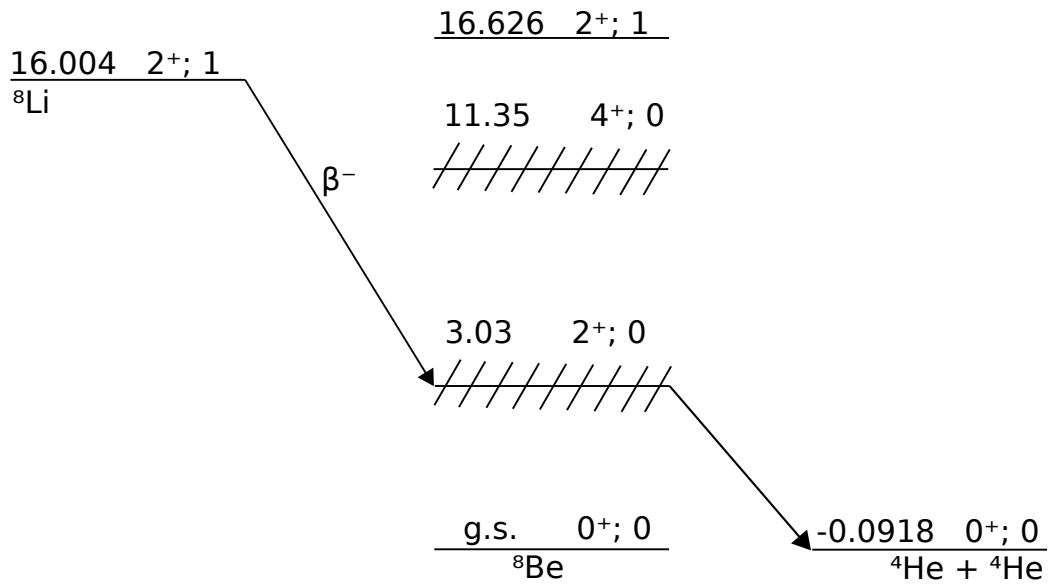


**Figure 1.1:** The decay scheme of  $^8\text{Li}$ , and some notable excitation energies of  $^8\text{Be}$ . Each level is labeled with the energy above the  $^8\text{Be}$  ground state in MeV. Spin parity and isospin is noted as  $J^\pi; T$ . All information is from [2].



## 2 Experimental Methods

The main goal of the experiment was to determine the  $\beta$ - $\alpha$  angular correlation. This ~~The experiment/It~~ was done at the IGISOL facility, at the University of Jyväskylä, where beams of all elements can be produced. The experiment took place in august 2020, due to a delay caused ~~delayed by the...~~ by the ongoing corona pandemic. This chapter will be concerning the experimental setup, a discussion of the detectors and an overview of the software used to extract and analyze the data.

### 2.1 Detector setup

The detection setup consists of 6 double sided silicon detectors (DSSD), and 6 single sided silicon detectors (SSD). The detectors are  $5\text{ cm} \times 5\text{ cm}$  and placed in a cube around the a target in the center, as shown on figure fig. 2.2. The setup is designed with measuring the opening angle of the  $\beta$  ~~beta-hvad? partikel?~~ in mind, and therefore the detectors covers 51% of the solid angle.

### 2.2 Experimental setup

The setup is designed to measure  $\beta - \alpha$  angular correlations in the  $\beta$ -delayed particle decay of  $^8\text{Li}$ . When measuring multiple particles, the setup is highly dependent on the coverage of the solid angle. Therefore the setup is designed to have a large solid angle coverage, with high  $\alpha$ -particle resolution, while still being able to measure  $\beta$ -particles. ~~Skal det eventuelt forklares ?~~

This is has been achieved by creating a cube of six double sided silicon detectors (DSSD) ~~Jeg tror bare du kan bruge DSSD her~~, all backed by a unsegmented silicon detectors (PAD). To gain the largest solid angle, the

detectors were placed as close to one another as possible. A 3D printed case was designed to hold the detectors in place, and achieved a solid angle coverage of 51% for the DSSD's, which can be seen on fig. 2.1. An illustration of the setup, together with the different detectors' thickness can be seen on fig. 2.2. Even though the setup was designed to hold 12 detectors in total, there were only 11 detectors in the actual experiment. The PAD behind Det1 was defect, and was therefore removed.

Detector	Thickness [ $\mu\text{m}$ ]	PAD	Thickness [ $\mu\text{m}$ ]
Det1	67	n/a	n/a
Det2	1002	P2	1036
Det3	65	P3	1497
Det4	60	P4	1490
DetU	60	PU	1498
DetD	1043	PD	1038

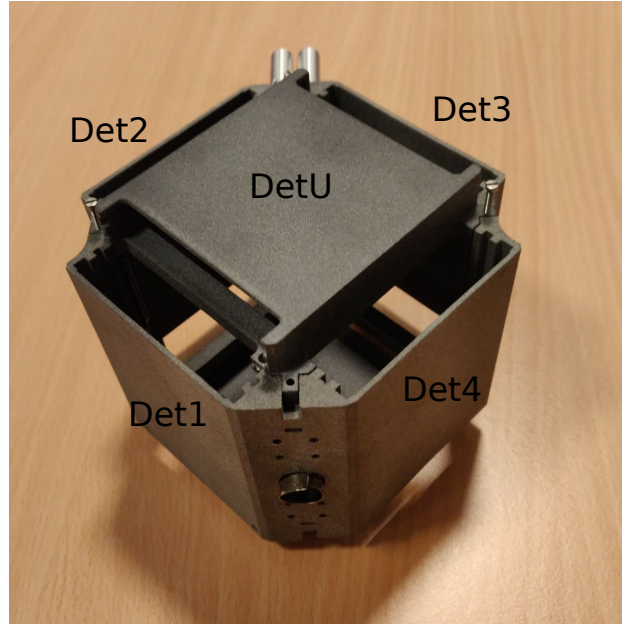


**Figure 2.1:** A picture of the 3D printed cube used to hold all detectors in place. The placement of the detectors have been shown, with exception of DetD, which was at the bottom of the cube. The beam enters the metal ring between Det1 and Det4

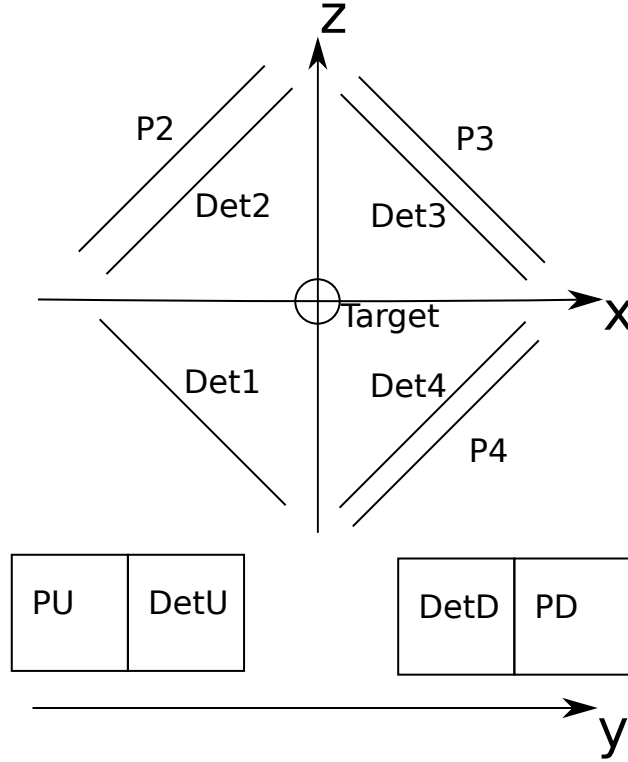


**Figure 2.2:** An illustration of the setup. Det1-Det4 are placed around the target, facing the target which is located at the center of the coordinate system. DetU are is above the target, and DetD are is below the target. Behind each detector is a PAD, with the exception of Det1, who's PAD was defect. The beam is parallel to the z-axis, entering the setup from the negative z-direction.

## 2.3 The detectors

As mentioned above, there where two types of detectors present in the setup. The first type is the Double sided silicon detector. As the name suggests, it consists of two sides, a front layer and a back layer. Each layer consists of 16 strips, that are placed in rows next to each other. The two layers are then arranged so each side are mutually orthogonal, which effectively makes pixels where each strip intersects a strip on the other side. An illustration of the detector can be seen on fig. [2.3](#).

The strips on the front side are p-doped, while the back side are n-doped.

When a charged particle hits the detector, it will ionize the atoms in the semi-conductor, and produce a electron-hole pair. The number of electron-hole pairs is proportional to the energy of the charged particle. The bias voltage on the detector collects the electrons and holes on opposite sites of the strip, where the charge is collected on aluminum contacts and a signal is measured. Energy is not deposited in these contacts, and therefore they constitute to a so called dead layer.

The detectors are square  $5 \times 5$  cm and with their  $16 \times 16$  strips, they have an effective gird of 256 pixels of 9 mm. 4 of the 6 detectors have a thickness of  $60 \mu\text{m}$  and a dead layer of 100 nm **dead layer**. These detectors are the ones called Det1, Det3, Det4 and DetU in the setup seen on fig. 2.2. The other 2 detectors (Det2 and DetD) where both  $1000 \mu\text{m}$ .

The other type of detector is the PAD. They are different from the DSSD's, in that they do not have sides, and no strips. Therefore they do not contain a grid, the same way the DSSD's do, and will not provide any information as to where a particle has hit. But they are included in the setup to detect excess energy of particles not stopped by the DSSD. This makes them good at detecting  $\beta$ -particles, as they will not be stopped by a DSSD.

An  $\alpha$ -particle will deposit all of its energy into the first DSSD it encounter, and be effectively stopped completely by it, and a  $\beta$ -particle will deposit almost no energy in a thin DSSD, and travel through it, ending up depositing some energy in the PAD.

Therefore one can roughly distinguish the  $\alpha$ -particles from the  $\beta$ -particles, by observing whether a particle has hit the DSSD and the PAD.

Since there are also two thick DSSD's in the setup, one can also get some information from a  $\beta$ -particle from these thicker detectors, as it will deposit more energy in these detectors.

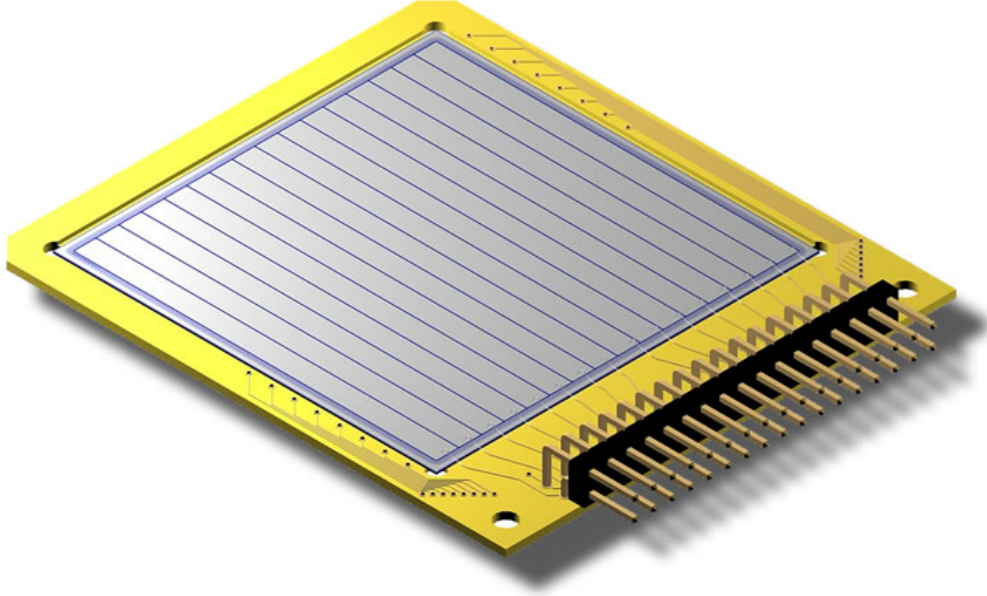


**Figure 2.3:** An illustration of the DSSD type used in this experiment. The detector has 16 p-doped strips, and 16 n-doped strips perpendicular to these. This gives 256 pixels for the detector. Image courtesy of Micron Semiconductor Ltd

## 2.4 AUSAlib and ROOT

ROOT [3] is an object oriented C++ framework that is designed primarily for data analysis in high-energy and nuclear physics. It was created at CERN in 1995, and has since grown and become the dominant analysis software at both CERN and many other nuclear and particle physics laboratories. ROOT was designed to handle large amounts of data with high computing efficiency.

ROOT makes an intelligent data structure by creating a "Tree" with the class `TTree`. This tree will then have "branches" which corresponds to some variable of the given detection event, such as the energy of the front strip or identity of the detector. This `TTree` skal det være texttt? then allows

for reading of an individual branch, while ROOT takes care of the memory management. One can also store a TTree to the disk in the form a .root file.

ASUALib [4] is a tool that build on top of ROOT. It was created by the subatomic group at Aarhus University. Before this tool was created, everyone in the group had to more or less create their own tools to get data from the detectors into a useful data structure. This meant that a lot of time was wasted just trying to access data from experiments. AUSAlib was therefore created, so the basic tasks of data extraction was automated.

AUSAlib has a lot of functionalities, but the two main tools that was used to extract data was the *Sorter* and *Calibrator*.

### 2.4.1 Unpacker

The **Unpacker** converts raw data from the detectors into a ROOT TTree. This is done by using the unpacking program `ucesb` [5]. This will setup the branch structure of the data. Some of these branches are FT and BT, which is a vector of the TDC (time) values for each event, for the front and backside of the detector. They are vectors because they contain information for each particle hits in a given time slot, for which there can be multiple. There are also the branches FE and BE, which is the ADC (energy) associated with the events.

### 2.4.2 Calibrator

Since the detectors work, by measuring an electrical charge that comes from the charged particle, the detectors needs to translate a specific charge to energy deposited.

To do that, we use the **Calibrator**-tool, which is designed to convert a channel number into an actual energy. Assuming that the channel numbers are linearly related to the energies, a known radioactive source can be measured, and the expected spectrum can be compared to the measured. This is done for each strip in each detector.

The **Calibrator** starts by running a peak-finding algorithm over some calibration data, to roughly identify the locations of the peaks, followed by a multi-Gaussian fit to find the most precise peak location. The positions of the peaks can then be compared to the expected energies, giving an associated energy to a given channel.

As mentioned earlier, all of the detectors have a small aluminum dead layer. All particles that pass through this layer will lose some amount of energy depending on the stopping power of the material and the effective thickness of the dead layer  $\Delta x_{eff}$ , which furthermore depends on the angle of incidence,  $\theta$ . The relationship between the effective thickness and the actual thickness is described as  $\Delta x_{eff} = \Delta x / \cos(\theta)$ . This gives the measured energy as

$$E' = E - \frac{dE}{dx} \frac{\Delta x}{\cos(\theta)},$$

where  $E$  is the original energy of the particle,  $dE/dx$  is the stopping power of the material and  $\Delta x$  is the thickness of the dead layer. The stopping power is calculated from SRIM [6]

These calculations are all handled by the **Calibrator**. As input it takes an unpacked measurement of a source, a file specifying the locations of the expected peaks and a file specifying the spacial locations of the detectors. From this it calculates the energy loss, and creates a linear relationship between channel numbers and energies. This is then written to the disk as a separate calibration file, which can be parsed to other modules.

It is important to note that the **Calibrator** does not modify any data. Therefore the energy loss is unaccounted for. Instead it corrects the expected energy spectrum, which means that the resulting calibration is still valid. The energy loss correction is therefore still needed in the analysis, as the effect is unaccounted for in measurements.

### 2.4.3 Sorter

The sorter is used after a successful calibration. It generates a ROOT file based on the unpacked data, and applies the calibration. It is also responsible for matching and combining events from the front-side to the back-side of the detector. If there were one hit in the front side and one in the back, the matching is fairly trivial. If there however were multiple hits in both front and back, the **Sorter** will run a matching algorithm, which pairs the hits with the lowest energy differences.

When the events have been matched, the hits on the individual sides of each detector are merged into a single event. Therefore each event can now be considered a multiple of particle hits. This makes it possible to associate physical properties with each particle, such as direction and energy. There has still not been done any filtering of the data, which is what we will discuss in [chapter 3](#).



## 3 Data Reduction

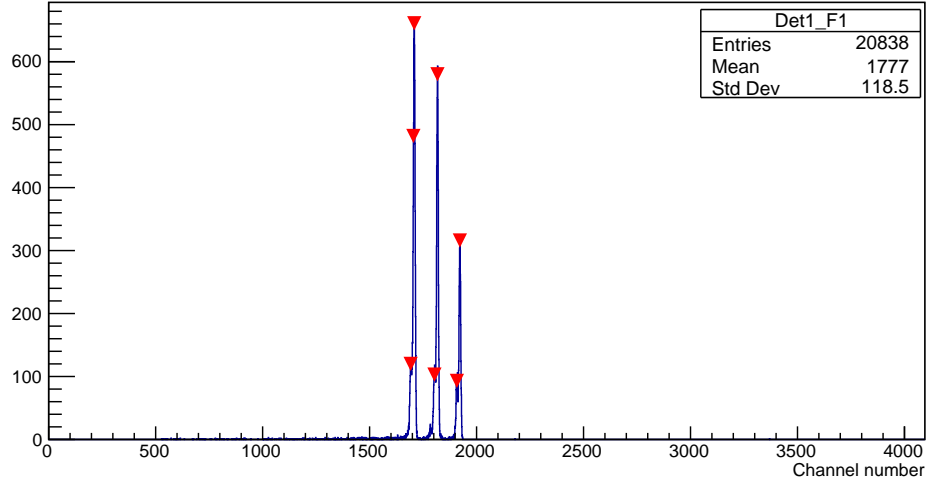
### 3.1 Calibration

To actually calibrate the detectors, we use an  $\alpha$ -source with a known spectrum. The source is placed in the target position, and each detector is in turn placed in front of the source. The radioactive source used to calibrate this setup contained  $^{148}\text{Gd}$ ,  $^{239}\text{Pu}$  and  $^{244}\text{Cm}$ . Each isotope has a prominent main peak, and several sub peaks. The proprieties of which is listed in table 3.1.

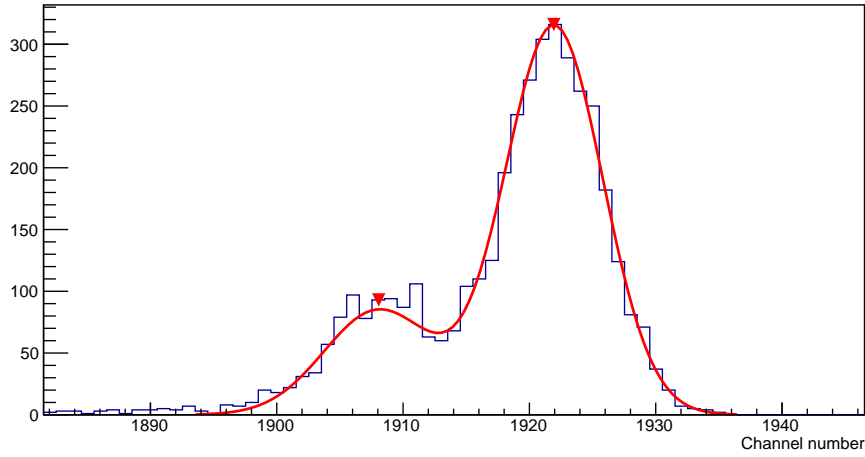
Isotope	$E_\alpha$ [keV]
$^{148}\text{Gd}$	3182.690
$^{239}\text{Pu}$	5105.5
	5144.3
	5156.59
$^{244}\text{Cm}$	5762.64
	5804.96

**Table 3.1:** Decay energies for each isotope used in the calibration.

A typical single strip spectrum is shown on fig. 3.1a, where the calibrator has given an estimate of where the peaks are, illustrated by the red triangles. fig. 3.1b shows a closer look at the  $^{244}\text{Cm}$  peak, where the red line shows the Calibrator-fit over both the main peak and the sub peak.



(a) A spectrum of the calibration source, with channel number along the x-axis. The red triangles indicate the positions the **Calibrator** has guessed as the peaks.



(b) A closer look at the  $^{244}\text{Cm}$  peak on the above figure. The red line is a fit performed by the **Calibrator**, and the red triangles indicate the guessed peaks.

**Figure 3.1:** Calibrations of detector 1

## 3.2 Identifying the particles

After utilizing the AUSAlib tools, the data is ready to be analyzed. Even though the theory dictates that a decay will consist of two  $\alpha$ -particles and one  $\beta$ -particles, it is not realistic to just assume that each detected event will consist only of this configuration of particles.

Therefore we need some cut on what events we will allow through to the analysis. Specifically we are going to impose 3 cuts on the data, a angular cut, a momentum cut and a multiplicity cut.

### 3.2.1 Identifying a hit

After a hit has been detected, and all the relevant information has been extracted from the hit, we can start to analyze what type of particle has hit the detector.

A important distinction between an  $\alpha$ -particle and a  $\beta$ -particle is the different interactions with a detector. An  $\alpha$ -particle will be completely stopped by a standard  $60\text{ }\mu\text{m}$  detector, while a  $\beta$ -particle will pass through it, depositing only a small amount of energy.

This is the reason for the PAD's behind each DSSD. The idea is that only a  $\beta$ -particle will be detected in the PAD's, so if a hit has some energy in a DSSD *and* the corresponding PAD, it will be classified as a  $\beta$ -particle.

This approach however does not work as well as intended. Often what happens is that the thin DSSD will not pick up any energy deposited, and the hit will therefore not be counted. But not all of the detectors are  $60\text{ }\mu\text{m}$ . We have two detectors that are around  $1000\text{ }\mu\text{m}$  thick. These detectors are much better at picking up a signal from a  $\beta$ -particle, so one of the criteria for being a  $\beta$ -particle in this setup is to have hit either Det2 or DetD.

These two criteria are however not enough to uniquely determine that a hit was a  $\beta$ -particle. We still have to consider the events where a detector has multiple hits. Since a PAD gives no usable information regarding where a particle has hit, we cannot say which particle was a  $\beta$ -particle and which where an  $\alpha$ -particle.

Therefore if the  $\beta$ -particle criteria are true, we mark the particle as a *possible*  $\beta$ . But since it might as well have been a  $\alpha$ -particle, we also mark it as such. Every hit that does not uphold to the  $\beta$ -particle criteria are of course marked only as a possible  $\alpha$ -particle.

When all the particles have been identified, we impose the first cut to the data. A multiplicity cut that says we need at least two  $\alpha$ -particles. If there are less, we discard the event.

When we at least have two distinct particles that can be  $\alpha$ -particles, we look at their mutual difference in momentum. The particle pair with the least difference in momentum will be chosen as the only  $\alpha$ -particles that can be present in an event. Then we have assured that every other particle we see in the event, is possible  $\beta$ -particle candidates.

When each particle has been identified or discarded, all remaining particle-specific information is stored to the given particle for easy analysis henceforth.

### 3.3 Angular cut

When  $^8\text{Be}$  decays, and produces the two  $\alpha$ -particles, it will do so under conservation of momentum. The decay in any direction, but the angle  $\theta$  between them will be close to  $180^\circ$ . Therefore the first cut that we give to the data, is that two of the particles that are  $\alpha$  candidates, must have a mutual angle of close to  $180^\circ$ .

On fig. 3.2 a plot of all the the mutual angles are shown. A quick glance will give that most particles will have mutual angle of close to  $180^\circ$ .

By looking at this, we see that most of the angles will lie close to  $180^\circ$ , and now we must decide exactly where to do the cutoff. By taking a sharp cutoff at  $\cos(\theta) \geq -0.99$ , we will exclude a great deal of good measurements, on the other hand, a too soft cut will not accomplish anything, as too many "wrong" particles will let through the check. By trying different cuts, we have found that  $\cos(\theta) \geq -0.95$  is a good cutoff, and this corresponds to  $161^\circ$ .

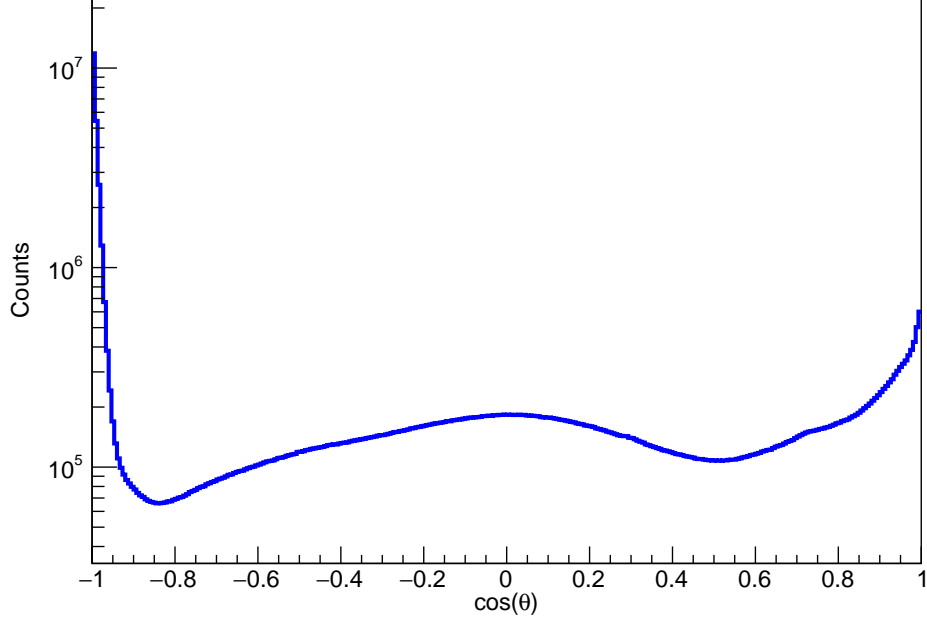


**Figure 3.2:** A histogram of all the mutual angles between all particles.

### 3.4 Momentum cut

The second cut we perform on the data is a *total* momentum cut. On fig. 3.3 the total momentum for the two identified  $\alpha$ -particles are shown. A prominent peak lies around 13.000 keV/c, and ends around 40.000 keV/c. We impose a cut of maximum 40 MeV/c, as this will include the large amount of pairs lying in the peak, which must be  $\alpha$ - $\alpha$  pairs. A  $\alpha$ -particle with energy 1500 keV will have a momentum of 105 MeV/c, and a free electron of 3000 keV will have a momentum of 1.7 MeV/c. The majority of particles lies around these energies, and no matter where the  $\beta$ -particle will hit, the total momentum is still much larger than the 40 MeV/c cutoff.

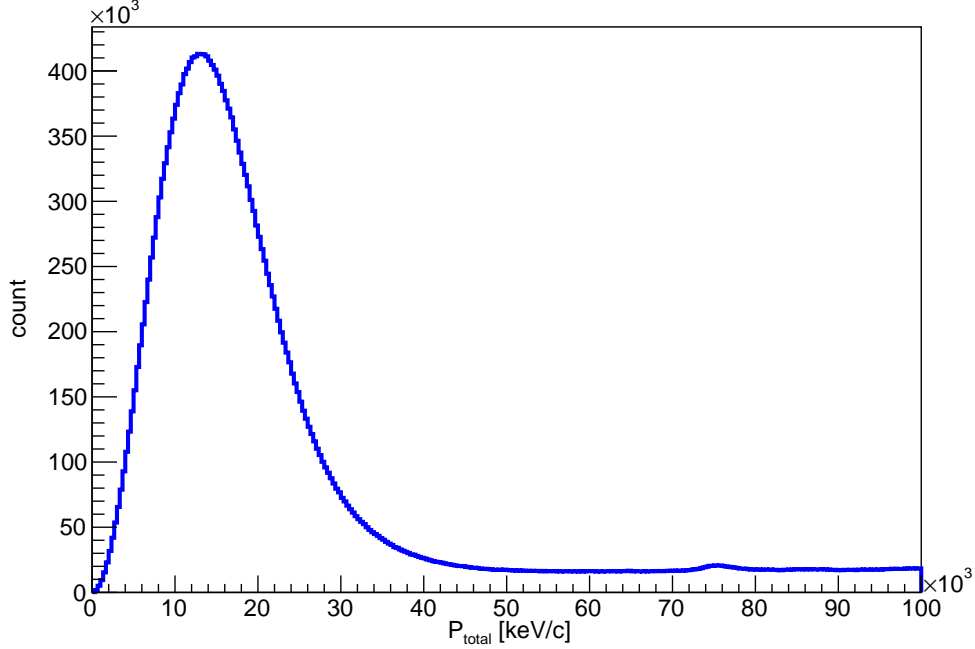


**Figure 3.3:** The total momentum of the two  $\alpha$ -particles.

### 3.5 Multiplicity cut

The last cut that we want to impose on the data, is a multiplicity cut. This cut is just to ensure that we have the amount of particles that we expect. Therefore a hard criteria is that there must be at least two distinctly identified  $\alpha$ -particles.

With regards to the  $\beta$ -particles, we are more loose. Here we say that there must at least be one, but more can occur. This is quite rare, but the we still take that event into account, as the  $\beta$ -particles should have an isotropic distribution, and therefore should not in any case be affected by the other  $\alpha$ -particles. On fig. 3.4 we see the multiplicity of  $\beta$ -particles, and in most of the events, we have not detected any  $\beta$ -particles, and when we do, there is a even fewer events with more than one beta. So most of the time, we are in the expected case with two  $\alpha$ -particle and one  $\beta$ -particle. add that beta

spreads around in the setup

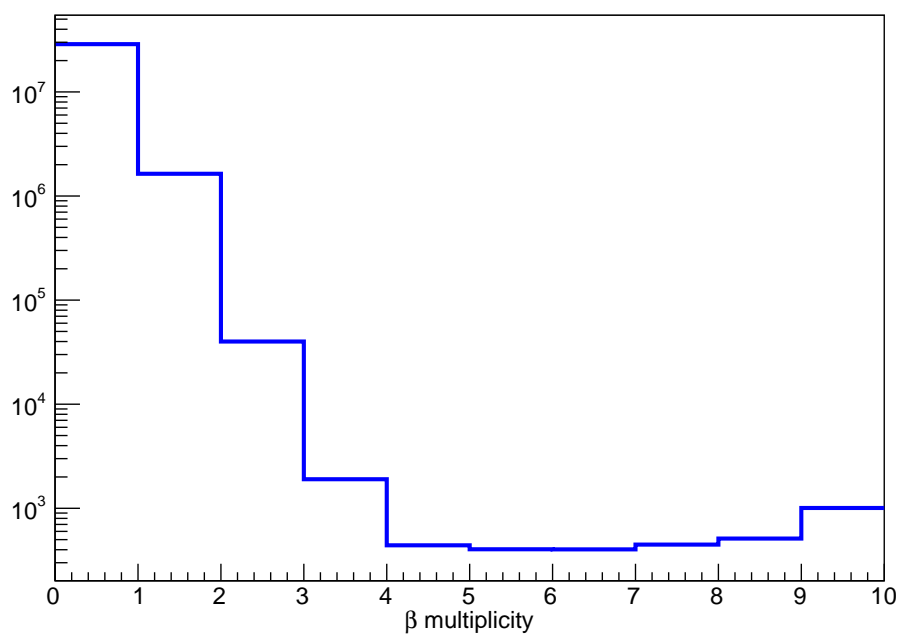


**Figure 3.4:** The multiplicity of the  $\beta$ -particles.

## 4 Analysis

### 4.1 The effects of the cuts

How does the cuts imposed in the previous chapter affect the data then? First we need to look at how the data looks, without any cuts. On fig. 4.1a the energy of the first  $\alpha$ -particle ( $E_{\alpha 1}$ ) is plotted against the energy of the second  $\alpha$ -particle ( $E_{\alpha 2}$ ). This gives us a nice view of what is considered  $\alpha$ -particle pairs. There is a prominent line going diagonally through the graph, where both particles have around the same energy. This line is expected, as the  $\alpha$ -particles will have close to equal energy, when decaying from  ${}^8\text{Be}$ .

This means that there is a lot of particle pairs that have been identified as  $\alpha$ - $\alpha$ , but properly was  $\alpha$ -noise, noise-noise,  $\alpha$ - $\beta$  or  $\beta$ - $\beta$  pairs.

The lines occurring from  $E_{\alpha 2} \approx 400 \text{ keV}$  are a clear example of a  $\alpha$ - $\beta$  pair. In this line,  $\alpha 1$  has been identified correctly as a  $\alpha$ -particle, which will have energies ranging from 500-6000 keV, whereas the the other particle has a more constant energy, corresponding to the energy a  $\beta$ -particle can deposit in a detector. So by doing no cuts at all, we are left with a lot of cases where we have no real control over what particle type we are dealing with.



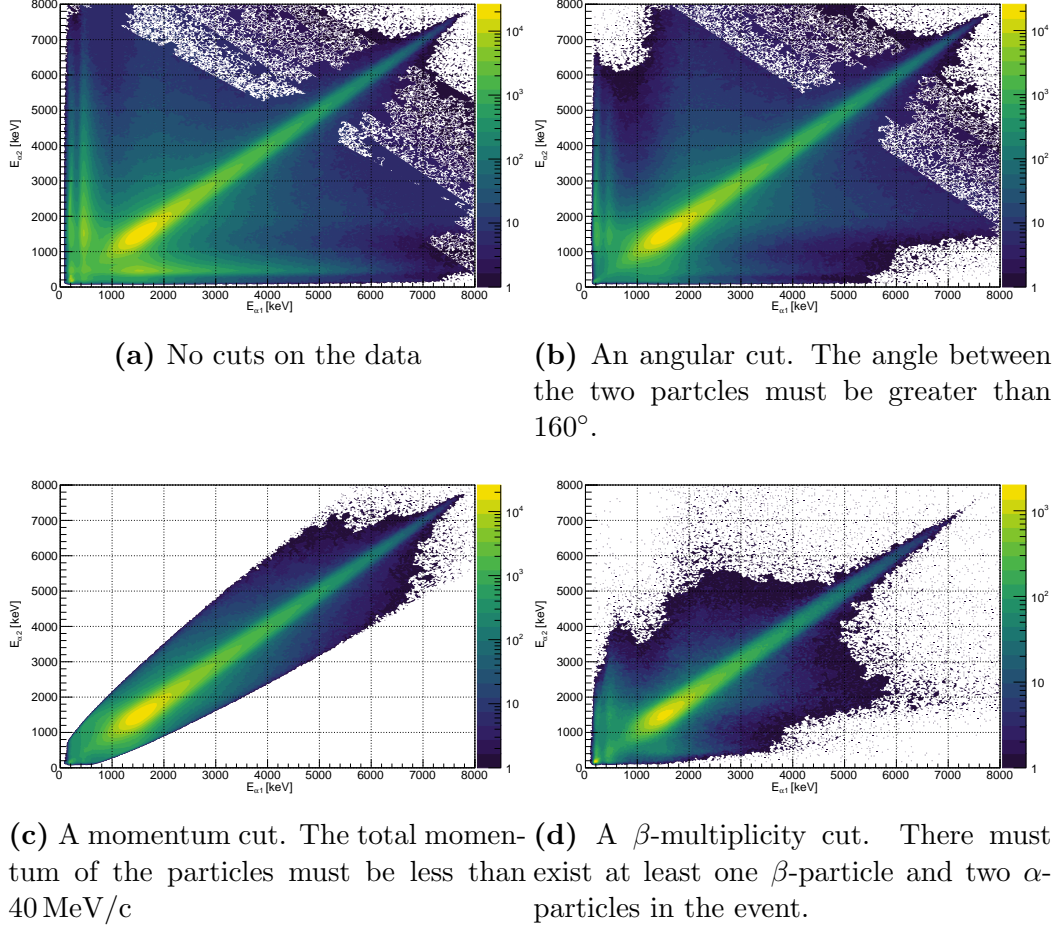


**Figure 4.1:** A collection of the different effects the cuts impose on the energy of the  $\alpha$ -particles. On all the above figures, the energy of the first  $\alpha$ -particle ( $E_{\alpha 1}$ ) is plotted against the energy of the second  $\alpha$ -particle ( $E_{\alpha 2}$ ). The intensity scale is in logarithmic, to get a better view of all the different particle configurations.

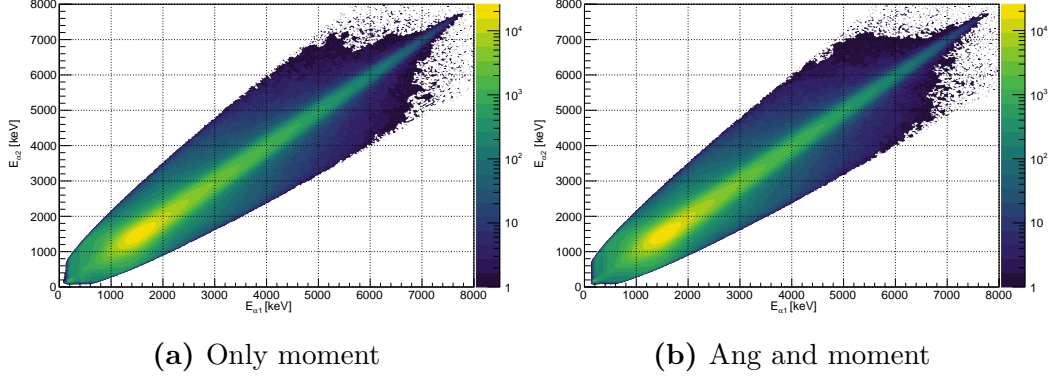


**Figure 4.2:** A comparison of the momentum cut with and without the angular cut.

#### 4.1.1 The effect of the angular cut

By imposing the angular cut, we get the first real reduction in data. If the angle between the two  $\alpha$ -particles are less than  $\cos(\theta) = -0.95 \approx 160^\circ$ , we sort away a good part of the  $\beta$ - $\alpha$  pairs, as seen on fig. 4.1b. But there are still a good portion of wrong pairs left, and we move on to impose a cut on the momentum of the particles.

#### 4.1.2 The effect of the momentum cut

Again the aim is to sort the data, so that we can identify the particles. On fig. 4.1c the total momentum of the two particles has been limited to a maximum of 40 MeV/c. This cut sorts away all of the vertical and horizontal lines from a  $\beta$ - $\alpha$  pair. With this drastic cut, it looks like there is no use for the angular cut, which might be true. On figure 4.2 we can see the comparison of the effect of the momentum cut, with and without an angular cut. There does not seem to be a very large difference. Since momentum already takes the direction of the particles into account, as well as their energies, the angular cut will seem a bit redundant. However, we keep the angular cut on the data, as it will not take away any "good" measurements, but only some noise that slips through the multiplicity cut. Looking at fig. 4.4, we see the blue line as the momentum cut and the magenta line as the momentum and angular cut.

The two histograms lie very close to each other, except in the low energy ranger. Here we see a slight reduction in the magenta line, indicating that the pure angular cut will sort some  $\beta$ -particles from the data. It is therefor a justified cut to still impose on the data.

### 4.1.3 The effect of the multiplicity cut

The multiplicity of the  $\beta$ -particles should not interfere so much with the  $\alpha$ -particles, but looking at fig. 4.1d, we see a drastic change in the pairs with energies far from each other. This is due to a general reduction in data. With the requirement that there must be one  $\beta$ -particle present in the event *and* that it must have hit either Det2 or DetD, we are left with a lot fewer measurements, which in turn gives a lower probability of noisy pairs.

### 4.1.4 The combined effect of all the cuts

By combining all of the cuts we are satisfied with the sorting of particles. On fig. 4.3 we see the effect of all the cuts. There is a very prominent line of particles with roughly the same energy. The line is thinner at higher energies, and widens as it goes towards lower energies. The reason for the widening, is the recoil energy from the  $\beta$ -decay. If the  $\alpha$ -particles have low energy, they are more susceptible to other forces around it, and will lose a larger portion of their energy to the  $\beta$ -particle recoil.

On fig. 4.4 all the cuts are shown as individually, highlighting the effect that each cut provides. Here it is worth noting that not all  $\beta$ -particles have been successfully removed from the data. A slight peak at low energies still remain for the black line in the figure. This is also clear on fig. 4.3, where there is a high intensity at the  $\approx 200$  keV energy range.

So far we have only considered that the  $\alpha$ -particles are sorted correctly. But there is still a question for weather the  $\beta$ -particles will be clouded by wrong identifications. On fig. 4.5 we see the energy deposited in the two detectors that are capable of measuring  $\beta$ -particles, and the pad behind Det2. The energy from the pad and DetD, shows one peak around 400 keV and 300 keV,

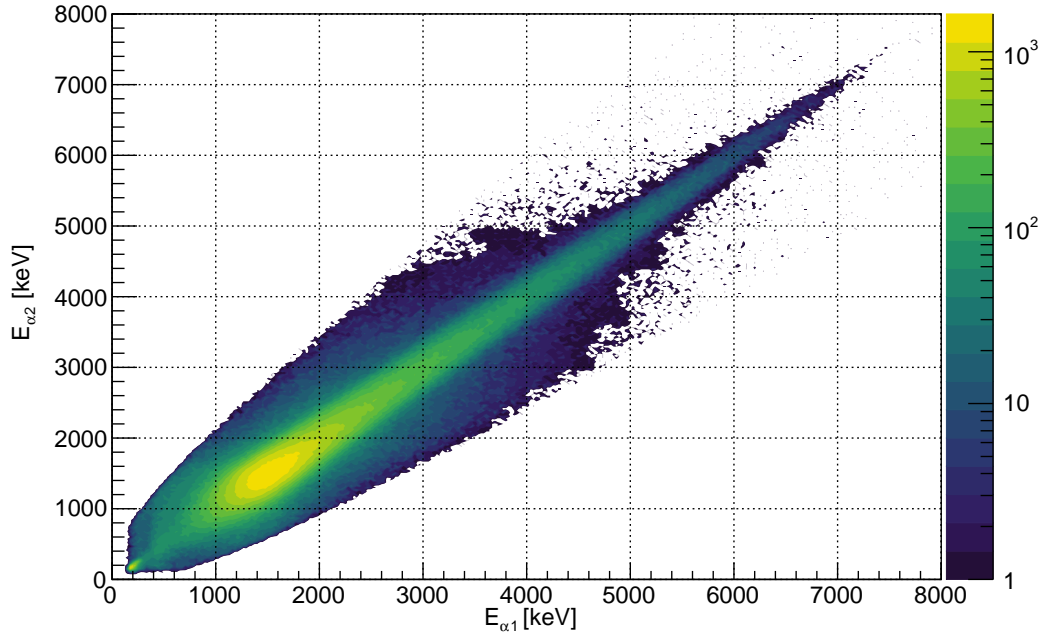


**Figure 4.3:** The energy of the first  $\alpha$ -particle plotted against the energy of the second  $\alpha$ -particle. All of the data reduction cuts are used here.

respectively. Det2 shows two peaks, one close to 400 keV, and one close to 800 keV. This is rather interesting, as we do not expect  $\beta$ -particles to deposit two different energies. Both detectors and the pad where 1000  $\mu\text{m}$  thick, so we expect that the energy deposited would be roughly the same.

## 4.2 The excitation energy of $^8\text{Be}$

With the  $\alpha$ -particles sorted correctly, we can start to look at the excitation energy of  $^8\text{Be}$ . All products of this decay will hit our detectors, and the entire energy of the decay can be measured. On fig. 4.6 the sum of both  $\alpha$ -particles energies are shown Er det et spektrum? Så kan de evt nævnes.

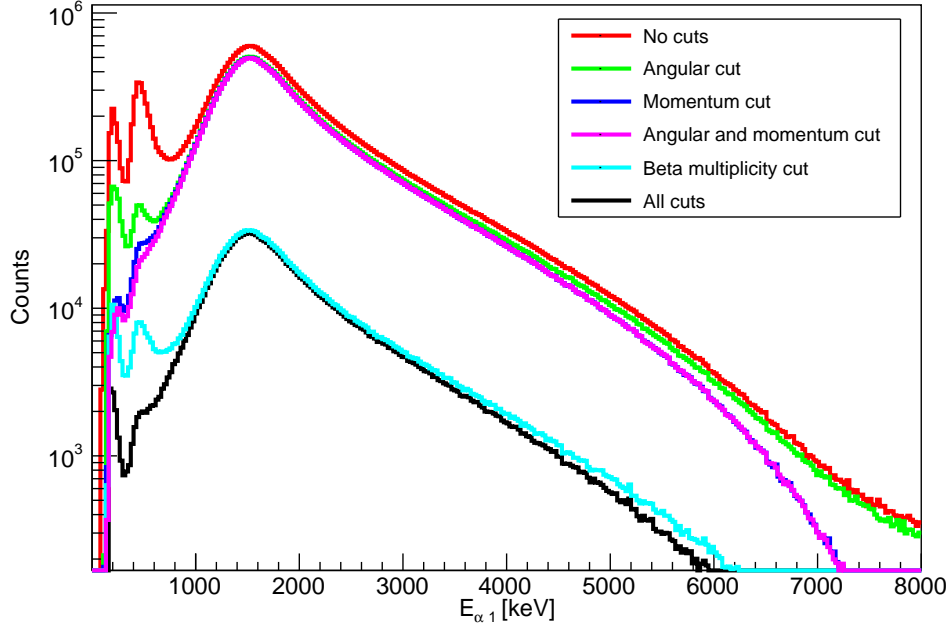


**Figure 4.4:** A comparison of all the cuts, where **with the energy...** the energy of the first  $\alpha$ -particle is plotted.

### 4.3 Angular efficiency of the setup

Since the detectors are unable to cover the entire solid angle, there will always be some mutual angles that are more likely to be measured. If we only look at one detector, a very large number of angles are not covered, but small mutual angles such as  $\theta \approx 0$ , are very easy to measure, as it is just a measurement of two particles in the same pixel. This effect becomes apparent on fig. 4.7, where the angular efficiency is shown for Det2. For a single detector, there cannot be angles of  $\theta = 90$  and higher, as the detector is flat. In this detector, the lowest angle found was  $\cos(\theta) = 0.21 = 77^\circ$  **Det er vist ikke rigtig notation.**

In this setup however, we **mangler et ord her** a cube of square detectors, who's normal vectors are all pointing in towards target at the center. This gives a much larger coverage of all mutual angles. The placement of the

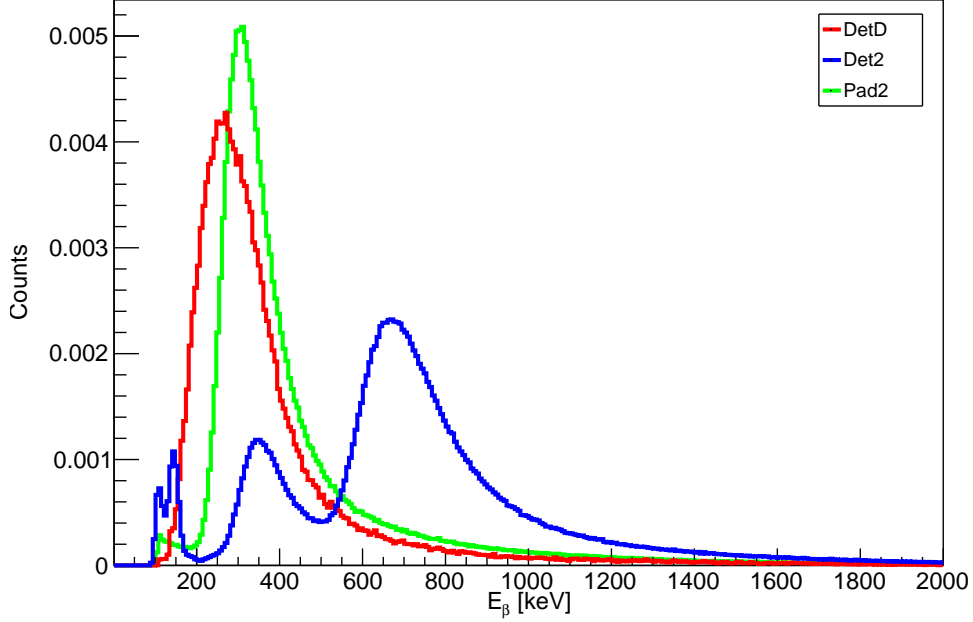


**Figure 4.5:** Energy deposited by  $\beta$ -particles in Det2 (blue), DetD (red) and Pad2 (green). PadD has been omitted, due to an error in the pad.

detectors gives that angles around  $\theta \approx 90^\circ$  are also very favored. This makes sense, almost no matter what pixel was hit, there is a corresponding pixel  $90^\circ$  to both sides. In the same way, will there always be a corresponding pixel  $\approx 180^\circ$  from each pixels. This effect can be seen on fig. 4.8.

This histogram was created by using the spacial coordinates of the entire setup. First the positions of each pixel in each detector was found. Then two loops running over each pixel pair  $i, j$ , finds the angle between these pixels and saves it ~~jeg ved ikke om man forstår dette hvis man ikke har været med til dette, så måske uddyb.~~

There is still a geometric effect that is not accounted for in the above analysis. We ~~måske slet~~ still - gentagelse still need to consider that not all pixels in the detector has the same effective area. The pixel furthest out in a detector will have a effective area smaller than the area of a pixel in the center. This effect can be seen on fig. 4.9a. Here we see that there is a much higher count

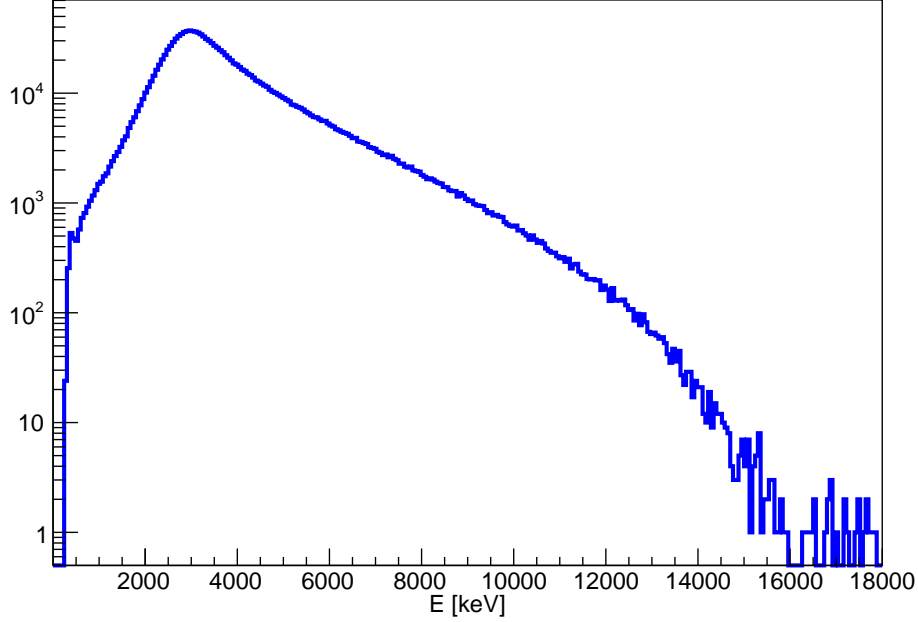


**Figure 4.6:** The energy spectra of both  $\alpha$ -particles, that is the excitation energy of  $^8\text{Be}$ . *Det forstår jeg ikke helt, skal det evt uddybes?*

of particles hitting the center of the detector, and fewer hitting the edges. A white line crossing through the middle is a defect strip, which did not measure anything. Sadly, some of the detectors had defect strips, but on a large scale it was not very noticeable *måske lidt vagt*.

To account for this effect *det lyder som om der referes til effekten af de døde strips*, each pixel will be associated with a corresponding area-efficiency ( $\text{Eff}_A$ ). This is calculated as

$$\text{Eff}_A = \frac{A \cos(\theta)}{4\pi r^2}, \quad (4.1)$$

where  $r$  is the distance to the pixel,  $A$  is the area of the pixel and  $\theta$  is the angle between the hit direction and the normal vector of the detector as shown on fig. 4.10. The area of all pixel is the same for all detectors, so the constants  $A$  and  $4\pi$  can be ignored when comparing the efficiency.

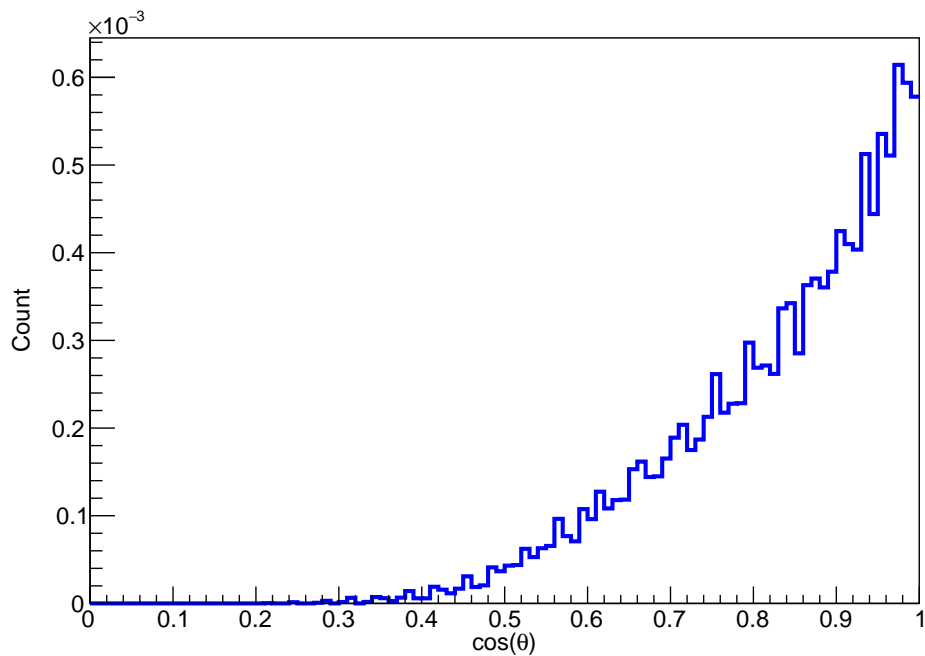


**Figure 4.7:** The angular efficiency of a single detector (Det2). For one flat detector, there can never be angles of  $90^\circ$  and higher.

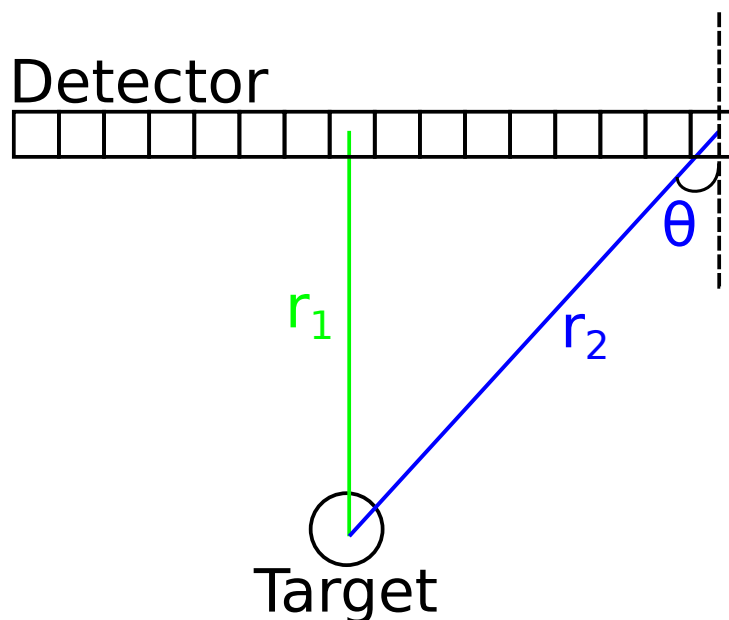


**Figure 4.10:** A illustration of two hits in different pixels. The blue hit will see a smaller effective area of the pixel by a factor determined by eq. (4.1) Måske tilføj "den blå retningsvektor projiceret på den stiplede linje bliver mindre for større theta eller noget". Denne figur er kommet i forkert rækkefølge



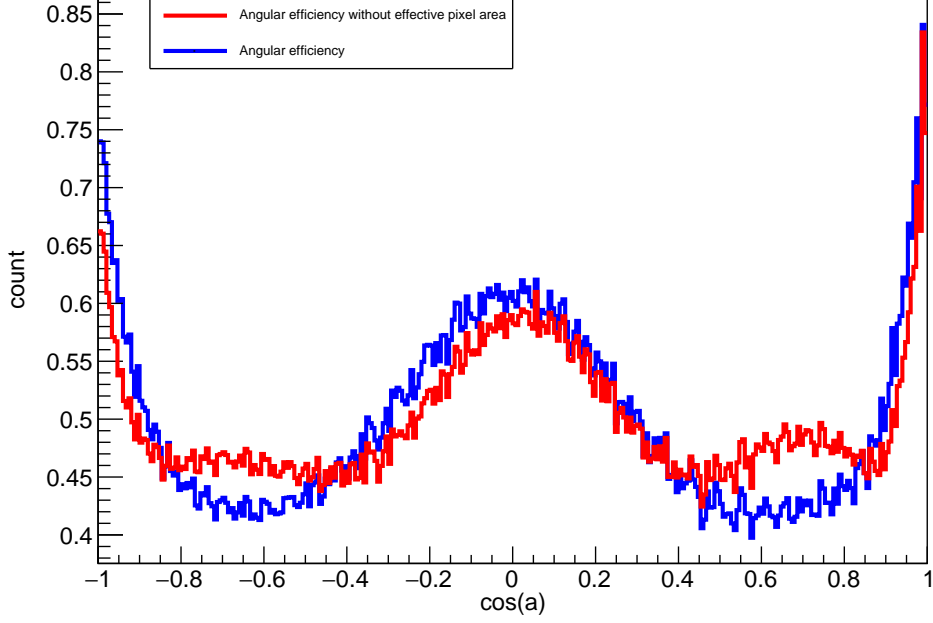
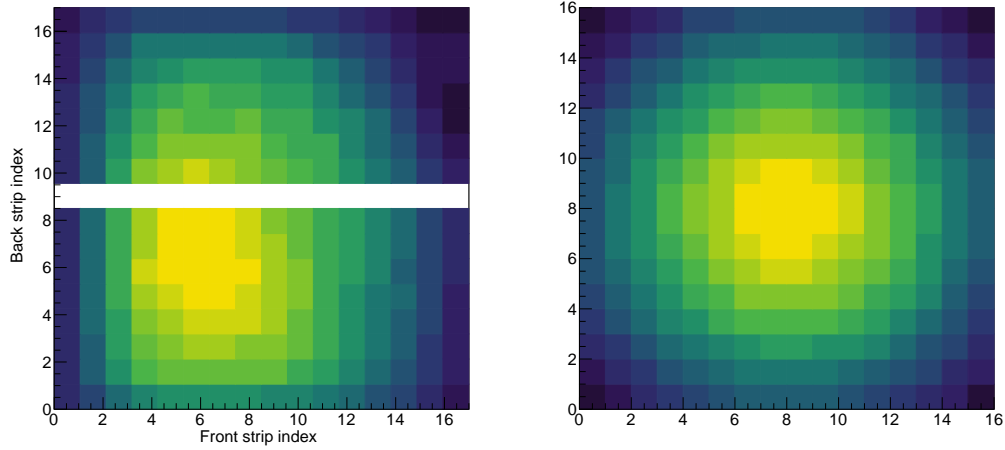


**Figure 4.8:** Two normalized histograms of the angular efficiency of the entire setup. The red histogram does not account for the effective area of a pixel. The blue is the true angular efficiency.

On fig. 4.8 two histograms can be seen. The red line represents the angular efficiency of the setup, without accounting for the relative area of the pixels, while the blue line is a weighted histogram for the same angles, with each pixels relative area accounted for.

The form of the two histograms are quite similar around 1, 0 and  $-1$  but in between there is a rather prominent difference. Therefore it is important that the effective area of the pixel is accounted for, when we in section 4.4 will look at the angular correlations of the  $\beta$ -particle in the setup.



(a) A plot over the number of hits in each strip for Det2. The white line in the middle is a defect strip, that did not measure anything.

(b) A theoretical intensity Det2.

Figure 4.9

## 4.4 Angular correlations of $\alpha$ -particles and $\beta$ -particles

From what we know in **ref til beta = isotrop** the  $\beta$ -particles must have an isotropic distribution. Since we only have two detectors in the setup that are capable of measuring  $\beta$ -particles, we cannot measure the angle from one particle to something constant, i.e. the beam. Therefore we measure the angle between both  $\alpha$ -particles and the  $\beta$ -particles. This is done by first finding the angle between the first  $\alpha$ -particle  $\alpha_1$  **vinkel mellem alfa og hvad?**, and create a histogram of this. Then the angle between the second  $\alpha$ -particle  $\alpha_2$  is measured **vinkel mellem alfa og hvad?**, and a histogram is created. The two histograms are then added, to get the full picture of the mutual angles of the particles. This can be seen on fig. 4.11 as the green line.

The blue line in this figure is the angular efficiency for the specific case, where the  $\alpha$ -particles can hit in any given detector, but the  $\beta$ -particles can only hit in the two specific detectors Det2 and DetD. The two histograms has both

been normalized, for a better comparison. By dividing the two histograms with each other, we get a better comparison. If they were to be close to equal, we would see a flat curve. But what we see on fig. 4.12 is not very flat. There are small fluctuations in the line, which stems from the inaccuracy of calculated angular efficiency. But the main shape of the curve is at most time not around  $y = 1$ .

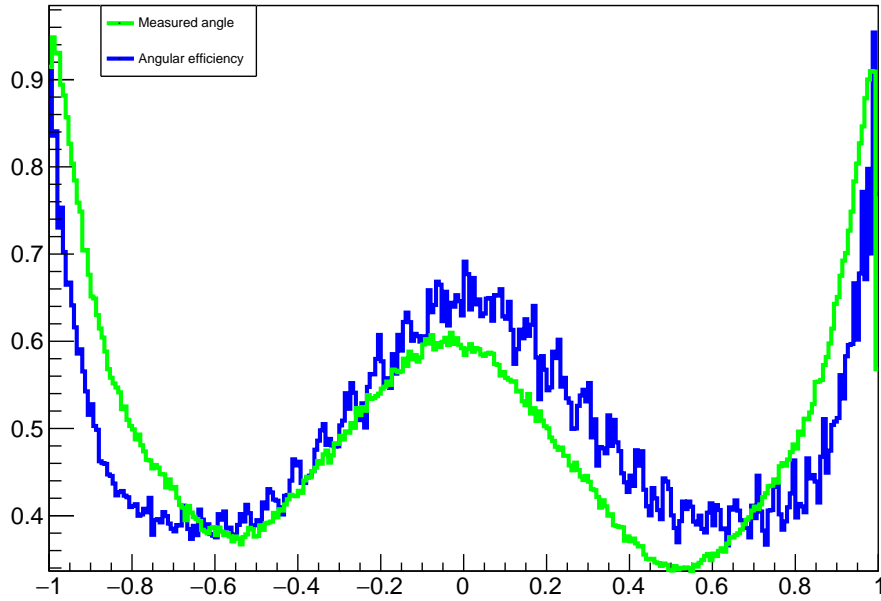


**Figure 4.11:** Some figure of the efficiency of the setup without efficiency of each pixel.

There are two different explanations as to why this might be. The first explanation is that the beam did not hit the target in the center. The calculated efficiency assumes that the beam hits precisely in the middle, but in any setup, there can be a few millimeters of errors.

By finding the angular efficiency of the setup, with different values for the center and comparing this to the measured angles, we have found a slight correction for the center of the beam. This can be seen on fig. 4.13a, where the beam has been moved to the coordinates  $(-3, -3, 0)$ , as opposed to the previous of  $(0, 0, 0)$ . The division of the two histograms on fig. 4.13b shows a

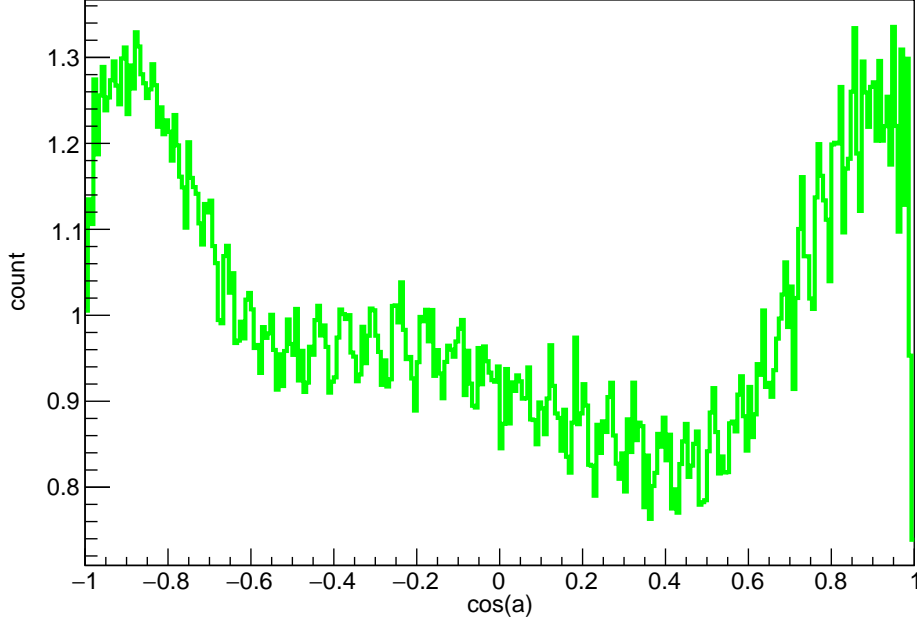
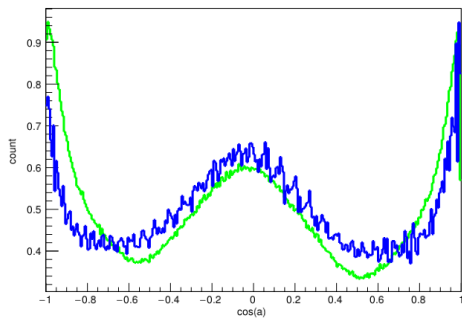


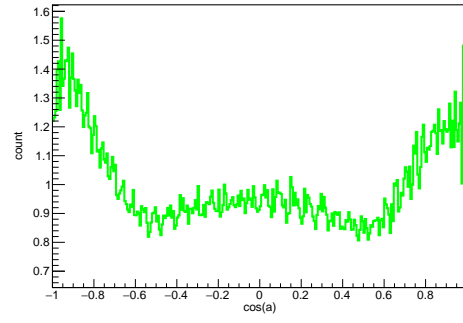
**Figure 4.12:** Data divided by the angular efficiency.

more stable line from  $\cos(-0.4)$  to  $\cos(0.4)$ , but the edges are still not very alike. Looking at  $\cos(1)$ , we see a rapid fall, which indicates that we have measured a lot fewer parallel  $\beta$  and  $\alpha$ -particles than the setup is designed to handle. This can be due to the fact that some of the strips were defect. The calculated angular efficiency does not know which strips were defect, and will therefore have a lot higher efficiency for parallel particles. The defect strips will therefore also play a role in the grand scheme, and is a possible explanation as to why there is a difference in the calculated and the measured data.

Another effect that will sway the data, is the target holder. This device will provide a shadow over the top and bottom detector, and since one of the  $\beta$ -detectors are the bottom one, it will skew the data in an unforeseeable way.



(a) The angular efficiency and the data, with a correction for the center of the beam.



(b) Measured  $\beta$ - $\alpha$ -particle angular distribution divided by the calculated angular efficiency of the setup, with a correction for position of the beam.

## 5 Conclusion

# Bibliography

- [1] R. E. Tribble and G. T. Garvey. Induced weak currents and  $\beta^\pm - \alpha$  angular correlations in  $a = 8$ . *Phys. Rev. C*, 12:967–983, Sep 1975.
- [2] D.R. Tilley, J.H. Kelley, J.L. Godwin, D.J. Millener, J.E. Purcell, C.G. Sheu, and H.R. Weller. Energy levels of light nuclei a=8,9,10. *Nuclear Physics A*, 745(3):155–362, 2004.
- [3] CERN. ROOT. <https://root.cern/>. 2021.
- [4] M. Munch, J. Halkjær, and O. S. Kirsebom. Ausalib - aarhus subatomic library. <https://git.kern.phys.au.dk/ausa/ausalib/wikis/home>, 2017.
- [5] ucesb. [fy.chalmers.se/~f96hajo/ucesb/](https://fy.chalmers.se/~f96hajo/ucesb/). Accessed June 8, 2021.
- [6] James F. Ziegler, M.D. Ziegler, and J.P. Biersack. Srim – the stopping and range of ions in matter (2010). *Nuclear Instruments and Methods in Physics Research Section B: Beam Interactions with Materials and Atoms*, 268(11):1818–1823, 2010. 19th International Conference on Ion Beam Analysis.